J|A|C|S ARTICLES

Published on Web 09/15/2010

Formation Mechanism of $CaTiO_3$ Hollow Crystals with Different Microstructures

Xianfeng Yang,[†] Junxiang Fu,[†] Chongjun Jin,[†] Jian Chen,[†] Chaolun Liang,[†] Mingmei Wu,*[,†] and Wuzong Zhou*[,‡]

State Key Laboratory of Optoelectronic Materials and Technologies, MOE Key Laboratory of Bioinorganic and Synthetic Chemistry, School of Chemistry and Chemical Engineering, School of Physics and Engineering, and Instrumental Analysis and Research Centre, Sun Yat-Sen (Zhongshan) University, Guangzhou 510275, P. R. China, and School of Chemistry, University of St Andrews, St Andrews, Fife KY16 9ST, United Kingdom

Received July 29, 2010; E-mail: ceswmm@mail.sysu.edu.cn; wzhou@st-andrews.ac.uk

Abstract: The crystal growth of $CaTiO_3$ hollow crystals with different microstructures has been investigated. In a water-free poly(ethylene glycol) 200 (PEG-200) solution, $CaTiO_3$ nanocubes formed first. The nanocubes underwent an oriented self-assembly into spherical particles, enhanced by the surface-adsorbed polymer molecules. Since the growth of nanocubes and their aggregation took place simultaneously, the nanocubes in the outer shells were larger than those in the cores. Disappearance of the small nanocubes in the cores of the spheres during an Ostwald ripening process led to spherical hollow crystals. Addition of a small amount of water (1.25 vol %) in the polymer solution enhanced surface recrystallization of the aggregated spheres, forming a cubic morphology. The orthorhombic distortion of the perovskite $CaTiO_3$ structure did not have a significant effect on the nanocube aggregation, resulting in a domain structure in the shells. Single-crystalline hollow cubes were produced with a slightly higher water content, e.g., 5 vol %. This process of (1) aggregation of nanocubes and (2) surface crystallization followed by (3) surface-to-core extension of recrystallization gives a good example of the reversed crystal growth route in ceramic materials. The proposed formation mechanism of the hollow $CaTiO_3$ crystals would enable us to control the microstructures of these materials and to explain the formation of many other hollow crystals.

Introduction

Control of crystalline phases, microstructures, and morphologies of inorganic functional materials continues to be a fundamental issue in modern materials science and technology.[1] Inorganic nanomaterials with hollow interiors have attracted great attention in recent years due to their widespread potential applications in many fields, e.g., new materials for sensors/probes, drug-delivery carriers, biomedical diagnosis agents, catalysts for size-selective reactions, etc.[2,3] To satisfy the different requirements of such applications, various hollow inorganic micro-/nanomaterials with different shell structural features, including their shapes, porosities, thicknesses, and crystallinity, were fabricated in the past few years.[3]

Besides traditional spherical hollow architectures composed of randomly aggregated or radially arranged building blocks, nonspherical hollow structures with well-defined regular morphologies have recently attracted more attention for their specific physical and chemical performances. Compared to the former, the nonspherical shapes are much more difficult to achieve by conventional templating methods, because suitable templates for a specific shape are often not available and the microstructures of the shells are less controllable.[4] Consequently, self-templating methods were extensively adopted in the synthesis of nonspherical hollow structures. For example, Yang et al. prepared rhombododecahedral silver cages through the Kirkendall effect by using rhombododecahedral Ag_3PO_4 crystals as sacrificial self-templates.[5] Polyhedral Cu_2O crystals have been widely used as sacrificial self-templates for growing copper sulfide hollow cages with nonspherical morphologies.[6] A variety of novel metal hollow architectures were fabricated by Xia and

[†] Sun Yat-Sen University.
[‡] St Andrews University.

(1) (a) Jun, Y. W.; Choi, J. S.; Cheon, J. *Angew. Chem., Int. Ed.* **2006**, *45*, 3414–3439. (b) Sayle, D. C.; Seal, S.; Wang, Z.; Mangili, B. C.; Price, D. W.; Karakoti, A. S.; Kuchibhatla, S.; Hao, Q.; Mobus, G.; Xu, X.; Sayle, T. X. T. *ACS Nano* **2008**, *2*, 1237–1251. (c) Wu, C. Z.; Xie, Y. *Chem. Commun.* **2009**, 5943–5957. (d) Yang, H. G.; Sun, C. H.; Qiao, S. Z.; Zou, J.; Liu, G.; Smith, S. C.; Cheng, H. M.; Lu, G. Q. *Nature* **2008**, *453*, 638–641. (e) Lee, I.; Delbecq, F.; Morales, R.; Albiter, M. A.; Zaera, F. *Nat. Mater.* **2009**, *8*, 132–138. (f) Qi, L. M. *Coord. Chem. Rev.* **2010**, *254*, 1054–1071.

(2) (a) Ma, Y. R.; Qi, L. M. *J. Colloid Interface Sci.* **2009**, *335*, 1–10. (b) Zeng, H. C. *J. Mater. Chem.* **2006**, *16*, 649–662. (c) Skrabalak, S. E.; Chen, J. Y.; Sun, Y. G.; Lu, X. M.; Au, L.; Cobley, C. M.; Xia, Y. N. *Acc. Chem. Res.* **2008**, *41*, 1587–1595. (d) Zhang, H. G.; Zhu, Q. S.; Zhang, Y.; Wang, Y.; Zhao, L.; Yu, B. *Adv. Funct. Mater.* **2007**, *17*, 2766–2771. (e) Yavuz, M. S.; Cheng, Y. Y.; Chen, J. Y.; Cobley, C. M.; Zhang, Q.; Rycenga, M.; Xie, J. W.; Kim, C.; Song, K. H.; Schwartz, A. G.; Wang, L. H. V.; Xia, Y. N. *Nat. Mater.* **2009**, *8*, 935–939. (f) Ye, L. N.; Wu, C. Z.; Guo, W.; Xie, Y. *Chem. Commun.* **2006**, 4738–4740.

(3) (a) Zhao, Y.; Jiang, L. *Adv. Mater.* **2009**, *21*, 3621–3638. (b) An, K.; Hyeon, T. *Nano Today* **2009**, *4*, 359–373. (c) Zhang, Q.; Wang, W. S.; Goebl, J.; Yin, Y. D. *Nano Today* **2009**, *4*, 494–507.

(4) Lou, X. W.; Archer, L. A.; Yang, Z. C. *Adv. Mater.* **2008**, *20*, 3987–4019.

(5) Yang, J. H.; Qi, L. M.; Lu, C. H.; Ma, J. M.; Cheng, H. M. *Angew. Chem., Int. Ed.* **2005**, *44*, 598–603.

co-workers also via self-templating routes.[7] These self-templating processes consist of two steps, first fabrication of precursors as sacrificial templates and then transformation to final hollow structures via the Kirkendall effect.

To avoid complicated operations, one-step template-free methods have also been widely employed for efficient production of nonspherical hollow structures. A general procedure of the template-free strategy can be described as (1) surfactant-assisted self-aggregation of primary building blocks and (2) development of the hollow interior via an Ostwald ripening process as observed in the formation of PbTe nanoboxes,[8] $CaTiO_3$,[9] and Cu_2O[10] hollow cubes. According to the previous reports, the shells of the as-obtained inorganic cage-like hollow architectures were mostly polycrystalline or built up by oriented aggregation of nanocrystallites. Detailed formation mechanisms of the aggregation and the microstructures of the shells have not been investigated extensively. In the present work, we focus on the formation mechanism of hollow crystals of $CaTiO_3$ with different microstructures in order to enrich our knowledge of this field of materials science.

The mineral perovskite $CaTiO_3$ is of both fundamental interest and practical importance in many disciplines such as mineralogy,[11] solid-state chemistry,[12] materials sciences,[13] electronic engineering,[14] and even biotechnology[15] due to its unique structure, easy fabrication, high stability, and biocompatibility. Much effort has been devoted to its synthesis, structural analysis, and application as an electronic or optical material. In our preliminary research, one type of $CaTiO_3$ hollow cage has been produced.[9] However, our knowledge of the formation of this hollow $CaTiO_3$ and other hollow crystals is still very limited. Herein, we report three different types of microstructured $CaTiO_3$ hollow crystals synthesized via a simple poly(ethylene glycol) 200 (PEG-200)-assisted solvothermal procedure but with varying small amounts of water in the solution. In particular, early stages of the crystal growth are studied, and a detailed formation mechanism of these hollow crystals is established.

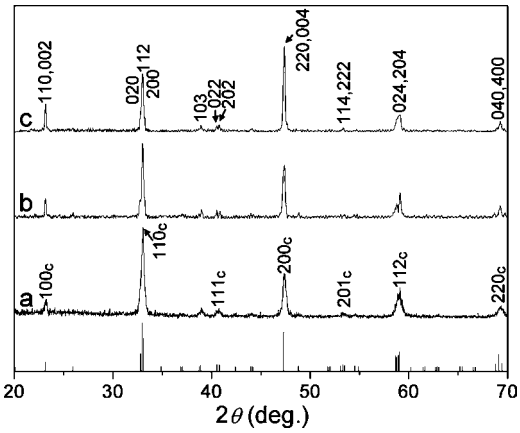

Figure 1. Powder XRD patterns of the $CaTiO_3$ specimens produced with different water contents in the synthetic solutions: (a) water-free, (b) 1.25 vol %, and (c) 5 vol %. The bottom pattern with vertical bars is derived from the JCPDS card (No. 82-0229, space group *Pbnm*) of orthorhombic $CaTiO_3$. Pattern (a) is indexed to the pseudocubic subcell with $a \approx 3.84$ Å, and pattern (c) is indexed to the orthorhombic unit cell with $a = 5.4033$, $b = 5.4406$, and $c = 7.6653$ Å.

Experimental Section

Synthesis. The synthetic method for $CaTiO_3$ hollow crystals was similar to that described in our previous report[9] with a minor modification. For sample I, 1.0 mmol of solid calcium nitrate, $Ca(NO_3)_2$, was directly dissolved in 19.67 mL of PEG -200 solvent without adding any water. An ultrasonic treatment was performed to enhance the dissolution of the calcium nitrate powder, and then 0.33 mL of tetrabutyltitanate [titanium *n*-butoxide, $Ti(OC_4H_9)_4$, TNB] was added dropwise into the solution under vigorous stirring, followed by addition of 22 mmol of sodium hydroxide powder under stirring to serve as the mineralization reagent. Subsequently, the mixture feedstock was transferred into a Teflon-lined stainless steel autoclave for solvothermal treatment at 180 °C for 15 h. The vessel was then cooled to ambient temperature. The precipitate was recovered by centrifugation, washed with acetone, diluted acetic acid, and distilled water, and then dried in a desiccator at ambient temperature.

For samples II and III, the precursor for Ca, $Ca(NO_3)_2$ powder, was replaced by aqueous $Ca(NO_3)_2$ solution (4.0 and 1.0 M, respectively). The volume ratios of $Ca(NO_3)_2$ solution to PEG-200 are adjusted to 0.25 mL (4.0 M):19.42 mL for sample II and 1.00 mL (1.0 M):18.67 mL for sample III, corresponding to water contents of 1.25 and 5 vol %, respectively, in the final solutions after addition of 0.33 mL of TNB. For examination of early-stage crystals, specimens after shorter reaction times, e.g., 1, 2, and 5 h, were also collected for each sample.

Characterization. The powder X-ray diffraction (XRD) patterns of the products were recorded with a Rigaku D/MAX 2200 VPC diffractometer using Cu Kα radiation ($\lambda = 0.15406$ nm) and a graphite monochromator. Scanning electron microscopy (SEM) images were taken using an FEI Quanta 400 Thermal FE scanning electron microscope. The samples for transmission electron microscopy (TEM) studies were prepared by dispersing the powder specimen on a holey carbon film supported on a copper grid, and the images were recorded on a JEOL JEM-2010HR electron microscope operated at 200 kV and equipped with a Gatan GIF Tridiem system.

Results and Discussion

The three samples produced with different contents of water in the synthetic solutions gave very similar XRD patterns as shown in Figure 1. All the diffraction peaks can be indexed to

(6) (a) Cao, H. L.; Qian, X. F.; Wang, C.; Ma, X. D.; Yin, J.; Zhu, Z. K. *J. Am. Chem. Soc.* **2005**, *127*, 16024–16025. (b) Jiao, S. H.; Xu, L. F.; Jiang, K.; Xu, D. S. *Adv. Mater.* **2006**, *18*, 1174–1177. (c) Zhang, W. X.; Chen, Z. X.; Yang, Z. H. *Phys. Chem. Chem. Phys.* **2009**, *11*, 6263–6268.
(7) (a) Chen, J. Y.; McLellan, J. M.; Siekkinen, A.; Xiong, Y. J.; Li, Z. Y.; Xia, Y. N. *J. Am. Chem. Soc.* **2006**, *128*, 14776–14777. (b) Lu, X. M.; Au, L.; McLellan, J.; Li, Z. Y.; Marquez, M.; Xia, Y. N. *Nano Lett.* **2007**, *7*, 1764–1769.
(8) Wang, W. Z.; Poudel, B.; Wang, D. Z.; Ren, Z. F. *Adv. Mater.* **2005**, *17*, 2110–2114.
(9) Yang, X.; Williams, I. D.; Chen, J.; Wang, J.; Xu, H.; Konishi, H.; Pan, Y.; Liang, C.; Wu, M. *J. Mater. Chem.* **2008**, *18*, 3543–3546.
(10) Teo, J. J.; Chang, Y.; Zeng, H. C. *Langmuir* **2006**, *22*, 7369–7377.
(11) Hu, M. S.; Wenk, H. R.; Sinitsyna, D. *Am. Mineral.* **1992**, *77*, 359–373.
(12) Mather, G. C.; Islam, M. S.; Figueiredo, F. M. *Adv. Funct. Mater.* **2007**, *17*, 905–912.
(13) (a) Lee, W. T.; Salje, E. K. H.; Goncalves-Ferreira, L.; Daraktchiev, M.; Bismayer, U. *Phys. Rev. B* **2006**, *73*, 214110. (b) Huang, Y. J.; Chiu, H. T.; Lee, C. Y. *CrystEngComm* **2009**, *11*, 1904–1909. (c) Huang, Y. J.; Tsai, M. C.; Chiu, H. T.; Sheu, H. S.; Lee, C. Y. *Cryst. Growth Des.* **2010**, *10*, 1221–1225. (d) Wang, D. A.; Guo, Z. G.; Chen, Y. M.; Hao, J.; Liu, W. M. *Inorg. Chem.* **2007**, *46*, 7707–7709. (e) Croker, D.; Loan, M.; Hodnett, B. K. *Cryst. Growth Des.* **2009**, *9*, 2207–2213.
(14) Wang, X. S.; Xu, C. N.; Yamada, H.; Nishikubo, K.; Zheng, X. G. *Adv. Mater.* **2005**, *17*, 1254–1261.
(15) Inoue, M.; Rodriguez, A. P.; Takagi, T.; Katase, N.; Kubota, M.; Nagai, N.; Nagatsuka, H.; Nagaoka, N.; Takagi, S.; Suzuki, K. *J. Biomater. Appl.* **2010**, *24*, 657–672.

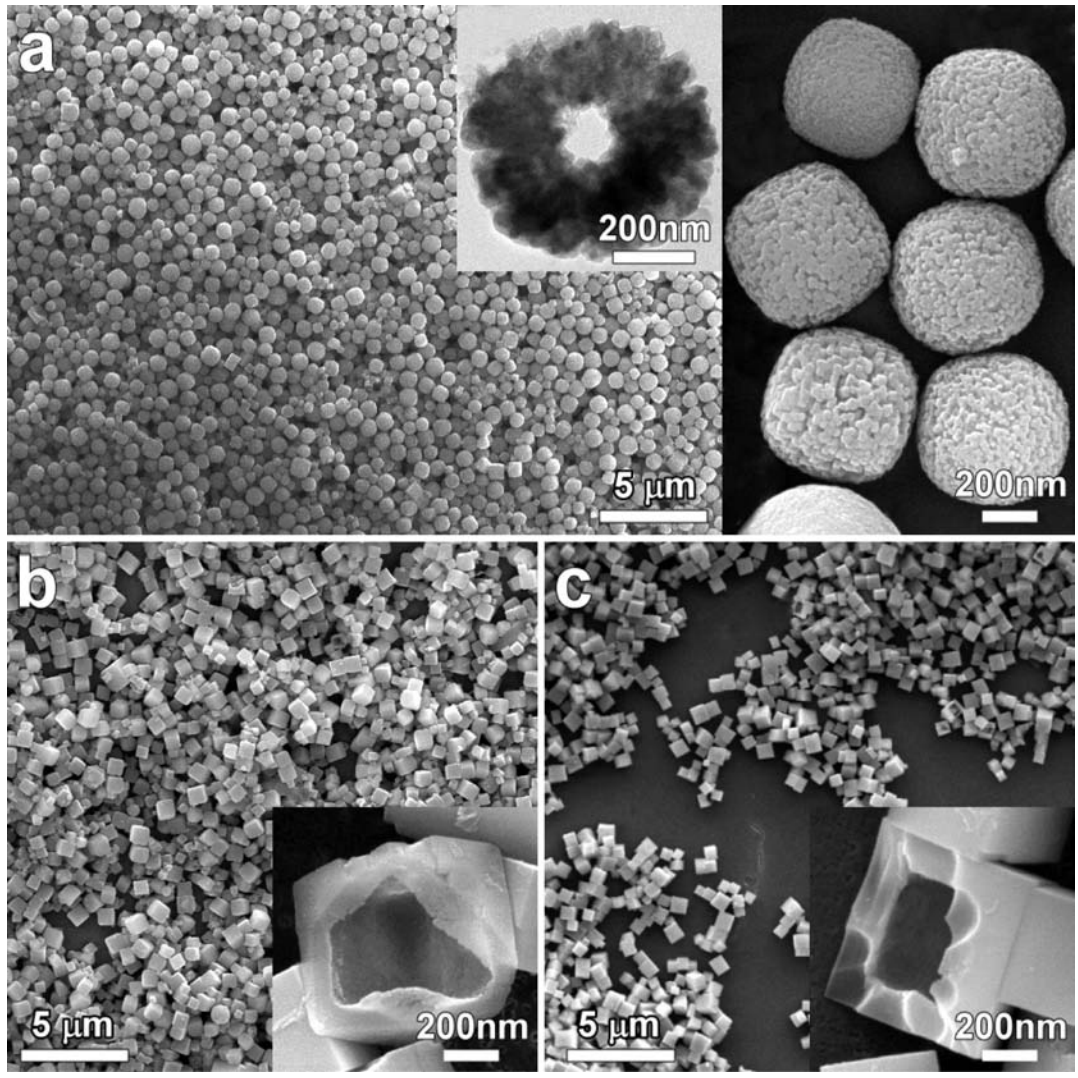

Figure 2. (a) Low-magnification SEM image of the as-synthesized $CaTiO_3$ product prepared in the water-free system. The inset in the middle shows a corresponding cross-section TEM image of a particle showing a hollow structure. The inset on the right side is a higher magnification SEM image showing the walnut-like surface. (b,c) SEM images of the cubic $CaTiO_3$ particles from samples produced in the 1.25 and 5 vol % water systems, respectively. The insets are corresponding SEM images of broken cubes, revealing the hollow structures.

the orthorhombic $CaTiO_3$ (JCPDS card No. 82-0229, unit cell $a = 5.4086$, $b = 5.4553$, and $c = 7.6782$ Å). Regarding the peak intensities, all the strong peaks can be indexed to a pseudocubic perovskite subcell with the cell dimension of $a \approx 3.84$ Å. The orthorhombic unit cell can be regarded as a $\sqrt{2} \times \sqrt{2} \times 2$ superunit cell based on the cubic perovskite subcell, leading to a cubic-to-orthorhombic transformation of the Miller indices, e.g., $(100)_c$ to (110), $(110)_c$ to (020), $(200)_c$ to (220), etc., where the subscript c denotes the cubic subcell. It is well known that the formation of the superstructure is due to regular tilting of the TiO_6 octohedra because the lattice tolerance factor (0.817) of $CaTiO_3$ is much smaller than 1 (Figure S1, Supporting Information). It is interesting to notice that the relative intensities of the $(100)_c$ and $(200)_c$ peaks of the sample obtained with 5 vol % water are significantly increased compared to those of the other two samples with less water in the synthetic systems.

SEM micrographs of the product shown in Figures 2a depict that the uniformly dispersed particles yielded from the water-free system have a walnut-like morphology with an average size of about 600 nm. The TEM micrograph of a thin slice of an individual particle clearly reveals a hollow interior with a shell thickness of about 200 nm (middle inset in Figure 2a). The shape of the particles is basically spherical. Figure 3 shows more detailed microstructure of these hollow particles. It can be seen that the walnut-like shells are piled up by nanocubes of about 40 nm in average size. The selected area electron diffraction (SAED) pattern from the whole hollow particle in Figure 3b shows that all the nanocubes are perfectly oriented according to the cubic subunit cell; i.e., all the nanocubes are connected with the $\{100\}_c$ faces. However, if the real orthorhombic unit cell is considered, the crystal orientations of the nanocubes are along three zone axes, $[\bar{1}10]$, [110], and [001], as described in Figure 4. The experimentally observed SAED pattern (inset of Figure 3b), although it looks like it results from a 2×2 superstructure based on the perovskite subunit cell, can be regarded as a combination of the three patterns, and only the three patterns, of the orthorhombic unit cell, corresponding to the orientations of $[010]_c$, $[100]_c$, and $[001]_c$ of the pseudocubic subunit cell.

To confirm the above conclusion, HRTEM images of several individual nanocubes were examined. For example, the HRTEM images and the corresponding FFT patterns of the marked areas in Figure 3b reveal that each cubic building block is a single crystalline orthorhombic $CaTiO_3$ with one of the above-

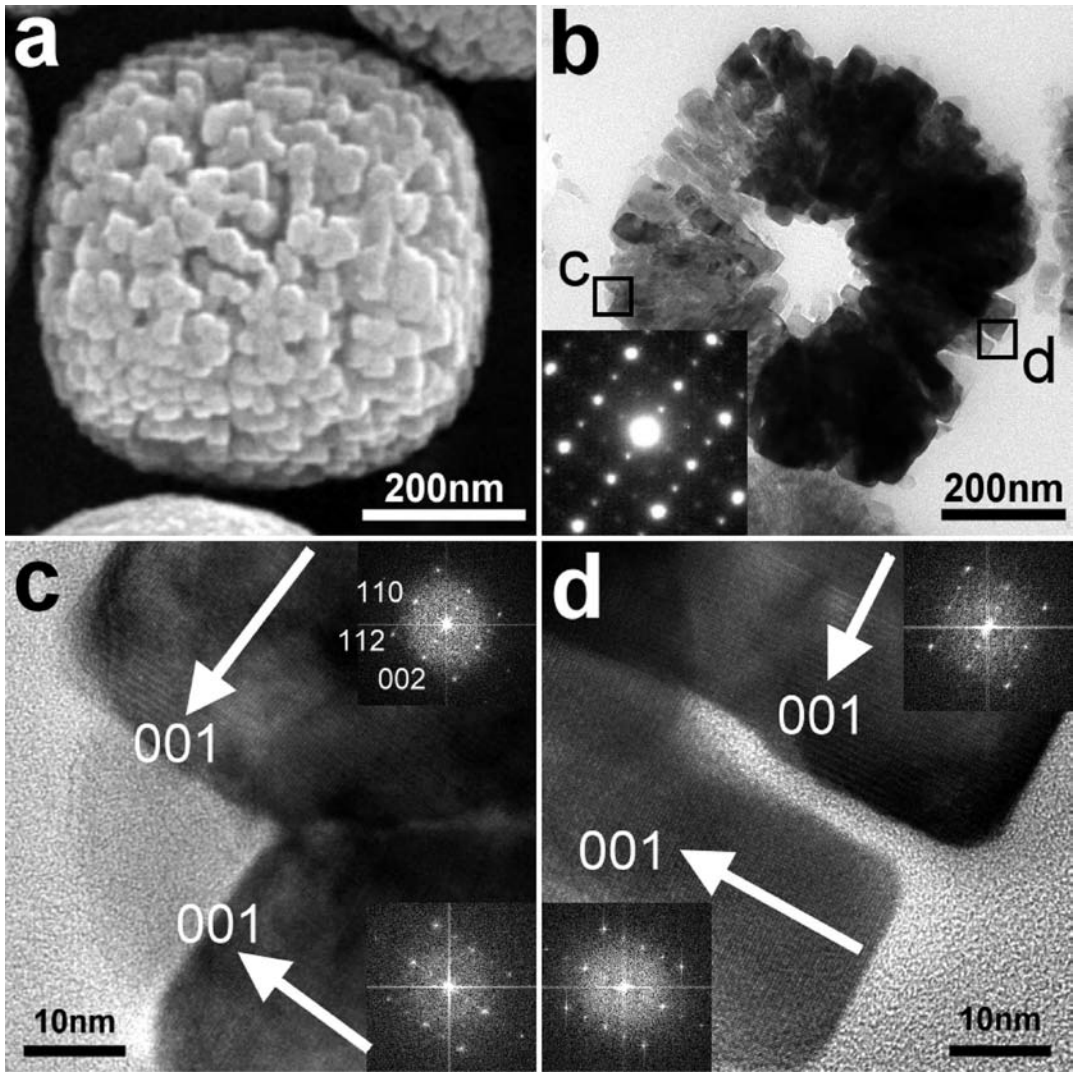

Figure 3. (a) SEM image and (b) cross-section TEM image of individual walnut-like $CaTiO_3$ particles produced in the water-free system. The inset of (b) is the corresponding SAED pattern from the whole hollow particle consisting of many nanocubes. (c,d) HRTEM images of the marked areas in (b) with the FFT patterns from individual nanocubes. The [001] axes of these nanocubes are indicated by arrows.

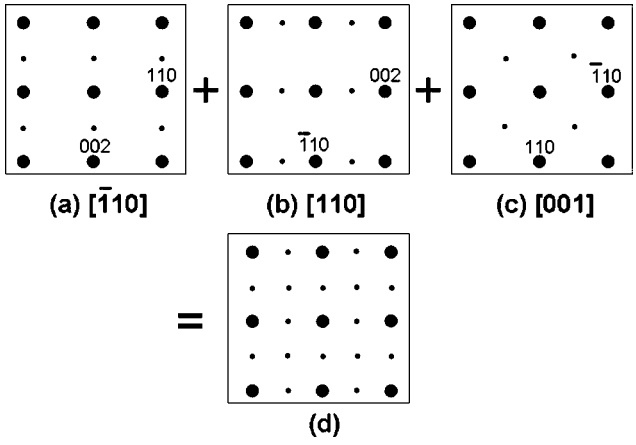

Figure 4. Schematic drawing to explain a combination of three SAED patterns (a−c) along the different zone axes of the orthorhombic unit cell of $CaTiO_3$ to result in (d) the SAED pattern shown in the inset of Figure 3b.

mentioned different orientations (Figure 3c,d). Such a microstructure and the formation of the nanocubes indicate that the orthorhombic distortion of $CaTiO_3$ due to the small lattice tolerant factor has little effect on the morphology of the monocrystalline nanocubes and the orientations of these nanocubes in aggregates. The formation of nanocubes with six $\{100\}_c$ facets implies that the minimum surface energies achieved by these facets along the three different axes are almost uniform. The particles behave like cubic crystals. The principal reason for such a phenomenon is that the difference in the adsorption of the PEG-200 molecules on these $\{100\}_c$ surfaces is not significant. Consequently, the adsorption of the PEG-200 molecules concealed the difference between these $\{100\}_c$ surfaces.

Compared to the walnut-like hollow particles obtained from the water-free system as described above, particles with a more regular cubic shape and smoother surface were fabricated by adding a small amount of water (e.g., 1.25 vol % for sample II and 5 vol % for sample III) into the system, with other reaction conditions unchanged (Figure 2b,c). Both the particle sizes and the uniformities are similar to those of the walnut-like particles in sample I. The broken particles clearly show they are also hollow, with larger empty cores.

The HRTEM images and SAED patterns show that the microstructures of these two samples are different. Figure 5a

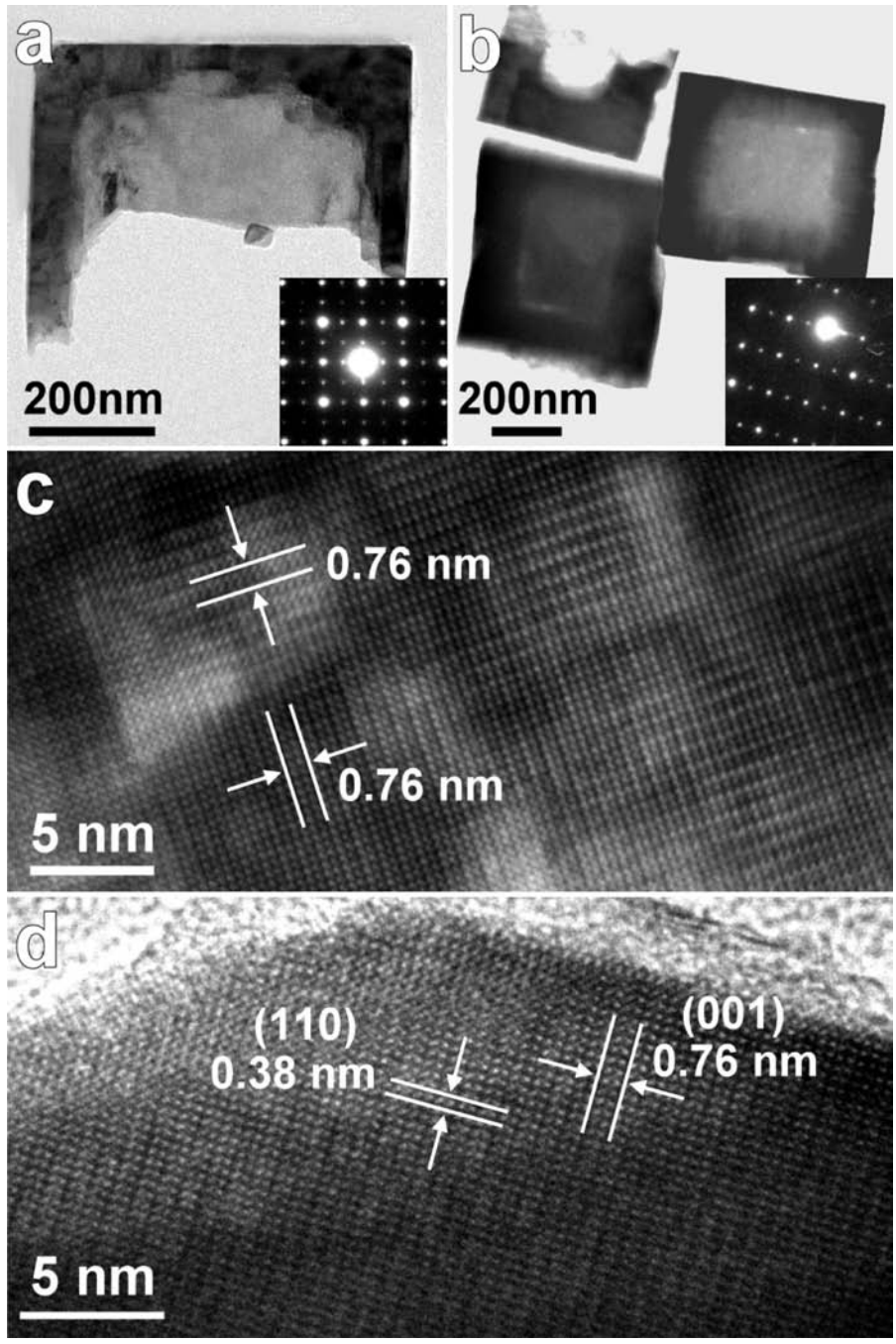

Figure 5. (a) TEM image of a broken hollow box from the specimen produced from the 1.25 vol % water system. (b) TEM image of specimen produced from the 5 vol % water system. The insets in (a) and (b) are the corresponding SAED patterns from the whole particles. (c,d) HRTEM images from the shells of the particles of the samples produced from 1.25 and 5 vol % water systems, respectively.

shows a TEM image of a broken hollow cube of sample II. The SAED pattern from a large area of the shell is very similar to that in the inset of Figure 3b, indicating a combination of three different diffraction patterns, as described in Figure 4. This conclusion is confirmed by a textured structure revealed by the HRTEM images of the shells as shown in Figure 5c. Consequently, the shells consist of nanodomains of orthorhombic $CaTiO_3$ with three different orientations, as mentioned in Figure 4.

In contrast, the shells of hollow cubes in sample III, prepared in the 5 vol % water system, are truly single crystalline, as seen from the SAED pattern of the inset of Figure 5b, recorded from a whole broken cubic particle. This SAED pattern can be perfectly indexed to the [110] zone axis of the orthorhombic unit cell of $CaTiO_3$, as shown in Figure 4a,b. The single crystalline property of sample III has been confirmed by HRTEM imaging, as shown in Figure 5d. Such well-oriented single crystalline hollow cubes with six $\{100\}_c$ facets, or four {110} and two {001} facets according to the orthorhombic unit cell, can explain why the intensities of the (110,002) and (220,004) peaks in its XRD pattern are higher than for the other two samples (samples I and II) (Figure 1).

To further investigate the formation mechanism of these hollow crystals, series specimens with shorter reaction times were collected in each synthesis. It is obvious that, in the water-free system for sample I, nanocubes of $CaTiO_3$ formed at an

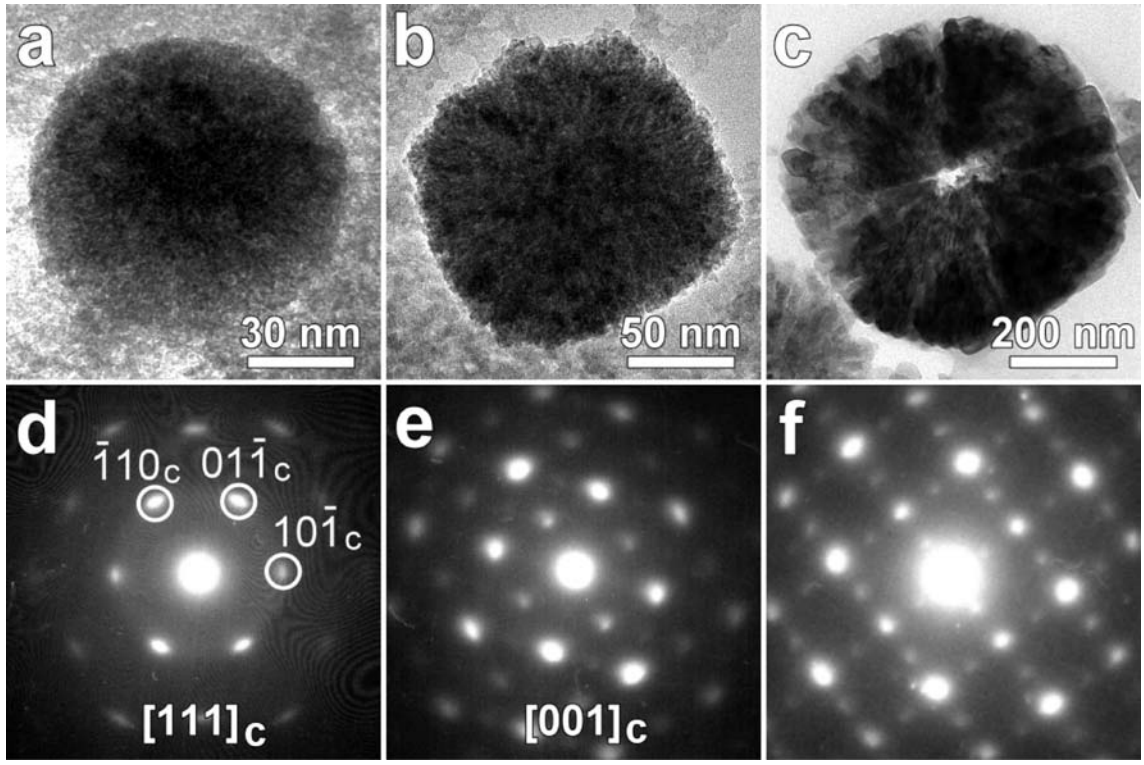

Figure 6. TEM images of particles in sample I obtained from the water-free system with different crystal growth times: (a) 1, (b) 2, and (c) 5 h. The corresponding SAED patterns are shown below (d−f).

early stage of the solvothermal process. The PEG-200 polymer molecules adsorbed on the $\{100\}_c$ surfaces of the nanocubes can enhance the oriented assembly of these nanocubes to form spherical aggregates, as observed in many similar processes, although the detailed mechanism is yet to be studied. Figure 6 shows TEM images of typical particles from specimens after reaction for 1, 2, and 5 h in the water-free system. It can be seen that the particle size increases with the reaction time from 90 nm (1 h) to 150 nm (2 h) and then 600 nm (5 h) in diameter. All the particles are aggregates of nanocubes which are about 40 nm or less in size. These polycrystalline particles are not hollow at first (Figure 6a,b), although many voids are presented randomly in the whole particles. A small hole was developed after reaction for 5 h (Figure 6c), which became much larger in the final product (Figures 2a and 3b). Another phenomenon we discovered is that the size of nanocubes in small aggregates is also small in comparison with that in larger aggregates. A natural consequence of the crystal growth in the solvothermal synthesis is that the potential for aggregation is so high that the growth of the nanocubes and their aggregation occur simultaneously. The growth rate of the nanocubes in the aggregates decreased significantly, leading to a gradual size increase of the nanocubes from the center to the surface of the walnut-like particles. The particles then underwent an Ostwald ripening process within a further thermal treatment when the relatively smaller nanocubes disappear to form hollow centers. The cage size increases with the time of the thermal treatment. At the same time, the density of the shells becomes higher when the size of the nanocubes increases, as estimated from the image contrast (see Figures 3b and 6c).

The SAED patterns from these particles are also displayed in Figure 6. It is obvious all the particles have almost perfect oriented aggregation. Moreover, smaller particles at earlier stages show less orthorhombic distortion from the cubic symmetry. Since cubic $CaTiO_3$ is a thermodynamically stable phase at temperatures over 1250 °C for bulk materials, it is interesting to note that it can be synthesized at much lower temperatures (180 °C) and exists at ambient temperature when the material is in nanoscale. Similar size-induced phase transformations have been previously observed in $BaTiO_3$ nanocrystals;[16] i.e., the smaller crystal size favors the cubic phase of $BaTiO_3$ rather than the tetragonal phase.

When a small amount of water (1.25 vol %) was added into the reaction system, the primarily formed nanocubes also underwent an oriented assembly to form spherical particles, as shown in Figure 7a. The SAED pattern of the particle in Figure 7a confirms the oriented aggregation regarding the pseudocubic subunit cell but random arrangement of three principal orientations according to the orthorhombic unit cell (Figure 7d). As the particle sizes increased with longer thermal treatment, the surface of the particles recrystallized, leading to morphology change from spheres to cubes. At this stage, the cubes are nonhollow (Figure 7b). As compared to sample I (Figure 6b), surface recrystallization was enhanced by an addition of water, which may reduce the number of adsorbed PEG-200 molecules on crystal surface and increase the solubility of the crystals, which helps recrystallization. The recrystallized surface of such a particle is believed to have a higher crystallinity or to contain some larger crystallites in comparison with the inner crystallites. Therefore, a following Ostwald ripening process will result in an extension of recrystallization from the surface to the core. Eventually, hollow cubes can form, as shown in Figure 7c. The cage volume further increased until the shell density approached the maximum value and the Ostwald ripening stopped (Figures 2b and 5a). The epitaxial intergrowth of the orthorhombic

(16) (a) Dutta, P. K.; Gregg, J. R. *Chem. Mater.* **1992**, *4*, 843–846. (b) Suzuki, K.; Kijima, K. *J. Alloys Compd.* **2006**, *419*, 234–242.

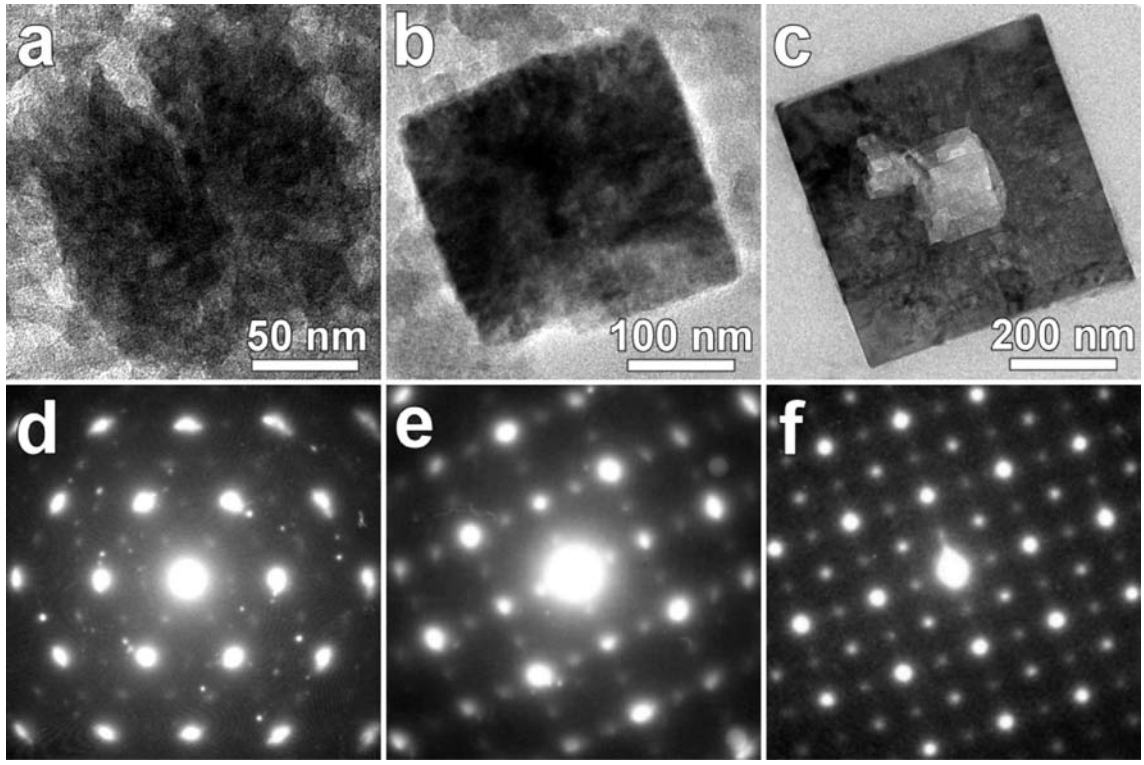

Figure 7. TEM images of particles in sample II obtained from the system containing 1.25 vol % water with different crystal growth times: (a) 1, (b) 2, and (c) 5 h. The corresponding SAED patterns are shown below (d−f).

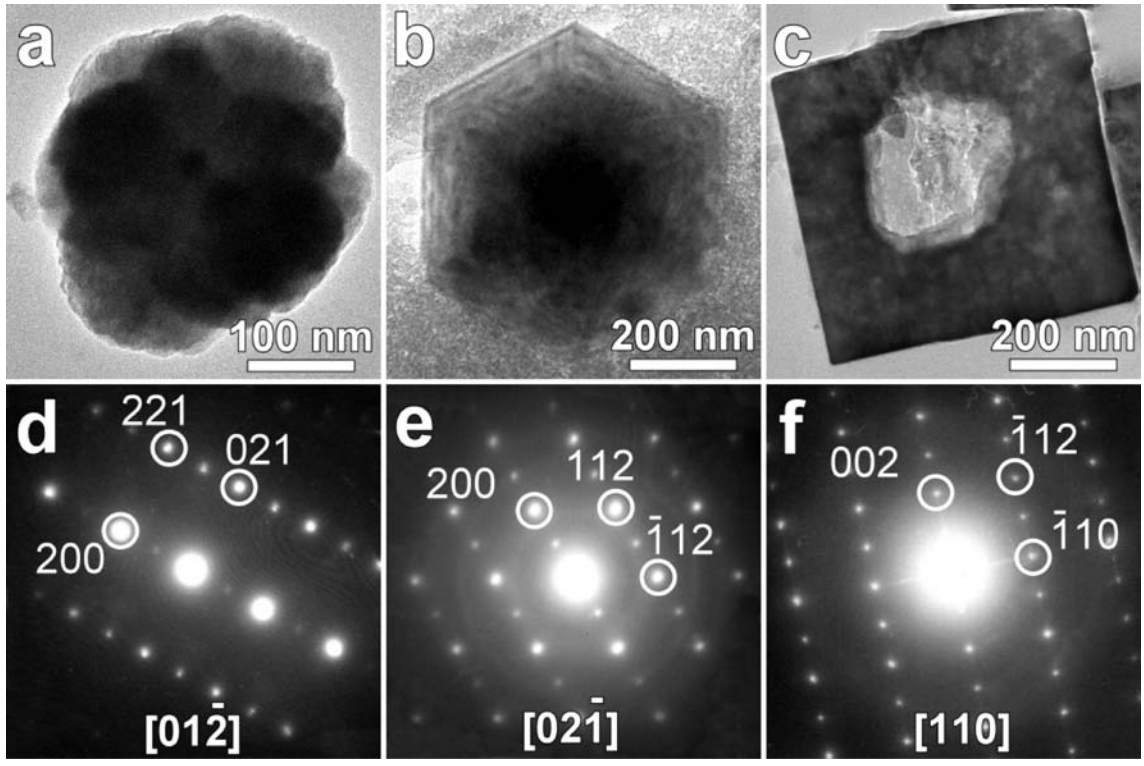

Figure 8. TEM images of particles in sample III obtained from the system containing 5 vol % water with different crystal growth times: (a) 1, (b) 2, and (c) 5 h. The corresponding SAED patterns are shown below (d−f).

$CaTiO_3$ domains or the textured structure (Figure 5c) was retained during the whole process of crystal growth.

In the 5 vol % water system, the development of the crystals in sample III was similar to that of sample II. The crystallinity of the former was much higher than the latter. A monocrystal-line-like property, regarding the orthorhombic unit cell of $CaTiO_3$, was detected by SAED (Figure 8d−f) for all the particles, even when the cubic morphology was not developed (Figure 8a). This indicates that water helped the nanocubes to aggregate with a perfect orientation according to the orthor-

Scheme 1. Schematic Illustration Showing Three Different Growth Mechanisms in (a) Water-Free, (b) 1.25 Vol % Water, and (c) 5 Vol % Water Systems[a]

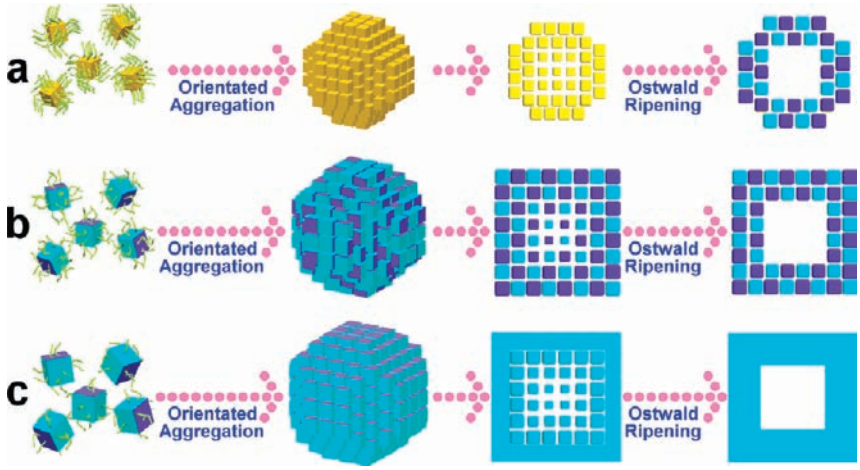

[a] The yellow cubes are cubic $CaTiO_3$. The light blue and dark blue cubes are orthorhombic $CaTiO_3$ particles with random orientations of $[\bar{1}10]$, [110], and [001].

hombic unit cell. Increasing the water content greatly suppressed the adsorption of PEG-200 molecules on the crystal surface and enhanced a better oriented aggregation of the nanocubes when the difference of the $\{100\}_c$ became obvious. Surface recrystallization followed by Ostwald ripening resulted in single crystalline hollow cubes, which was also confirmed by HRTEM studies (Figure 5d). It was noticed that, similar to sample II, the outer surface of the cubic shells is smooth, while the inner surface is quite rough.

The experimental results obtained in the present work clearly demonstrate the formation mechanisms of the $CaTiO_3$ hollow crystals as illustrated in Scheme 1. The nanocubes of $CaTiO_3$ form at an early stage in all three synthetic systems. In the water-free reaction system for sample I (Scheme 1a), the nanocubes undergo an oriented aggregation according to the pseudocubic subunit cells enhanced by the polymer PEG-200, which conceals the difference of the surface energies of $\{100\}_c$. Therefore, according to the orthorhombic unit cell, the intergrown faces are randomly (110), $(1\bar{1}0)$, and (001). The sizes of the nanocubes in the nonhollow spherical aggregates increase from the center to the surface. An Ostwald ripening process then leads to the disappearance of smaller nanocubes in the central area, forming hollow walnut-like hollow particles. When 1.25 vol % water is added for sample II (Scheme 1b), a surface recrystallization takes place in the spherical aggregates of the nanocubes to form a high-density cubic shell with a textured structure. Since the surface of the walnut-like particles in sample I was not recrystallized into a single-crystal shell, gaps between the nanocubes were obvious, as seen in SEM and TEM images (Figures 2a and 3). A textured structure was developed during surface recrystallization in sample II. Therefore, the grain boundaries were very fine and could only be observed in HRTEM images (Figure 5c). Sample III had a true single-crystal shell without grain boundaries. Water plays an important role in recrystallization that extends from the particle surface to the cores via an Ostwald ripening process. A hole forms eventually in the center of each particle. If 5 vol % water is added in the reaction system for sample III (Scheme 1c), it not only enhances the surface recrystallization to form a cubic morphology but also facilitates self-adjustment of the orientations of the nanocubes, resulting in oriented aggregation according to both the pseudocubic subunit cell and the real orthorhombic unit cell.

Conclusions

The phenomenon of surface recrystallization followed by an extension of recrystallization from the surface to the core of a polycrystalline aggregate is similar to the reversed crystal growth of some zeolites previously reported by one of the authors, Zhou and co-workers.[17] In Zhou's recent publication, the general mechanism of the crystal growth is discussed.[18] At a very early stage of crystal growth, there is a competition between the aggregation and growth processes. If crystal growth is fast, individual crystallites quickly approach a certain size, at which aggregation becomes difficult. This is the classic growth route. If aggregation occurs before the crystals become too large due to a strong van de Waals interaction between the chemical building units, the crystal growth of individual crystallites is suppressed. Surface recrystallization of the aggregated particles will take place, and the reversed crystal growth route will be followed. Zhou predicted that the hollow $CaTiO_3$ cubes shall form with a mechanism similar to the latter route, i.e., the reversed crystal growth route, as for the formation of hollow cubes of zeolite A. A time-dependent investigation would reveal more details. The present work confirms this prediction and demonstrates the first ceramic example of the reversed crystal growth. It shows again that when aggregation dominates in the early stages of crystal growth, the classic theory of crystal growth may not be followed. A single crystal may not be developed from a single nucleus, and its regular polyhedral morphology may not be directly related to the different crystal growth rates along different zone axes. Surface recrystallization of polycrystalline aggregates will select a morphology to keep a minimum surface free energy, as predicted by Curie and Wulff

(17) (a) Chen, X. Y.; Qiao, M. H.; Xie, S. H.; Fan, K. N.; Zhou, W. Z.; He, H. Y. *J. Am. Chem. Soc.* **2007**, *129*, 13305–13312. (b) Yao, J. F.; Li, D.; Zhang, X. Y.; Kong, C. H.; Yue, W. B.; Zhou, W. Z.; Wang, H. T. *Angew. Chem., Int. Ed.* **2008**, *47*, 8397–8399. (c) Greer, H.; Wheatley, P. S.; Ashbrook, S. E.; Morris, R. E.; Zhou, W. Z. *J. Am. Chem. Soc.* **2009**, *131*, 17986–17992.
(18) Zhou, W. Z. *Adv. Mater.* **2010**, *22*, 3086–3092.

100 years ago.[19] This mechanism can be used to explain the formation of many other hollow crystals, including some natural minerals. For example, some precious agate stones have a hole inside with or without liquid, the latter being often called water agate. These agate stones may form via the reversed crystal growth, similar to what we observed in the present work. The better understanding of the formation of the hollow crystals will enable us to control the syntheses of these materials for various applications.

Acknowledgment. We gratefully thank Dr. Yanbin Wang at the University of Chicago and Dr. Qisheng Huo at Jilin University for their fruitful discussions. This work was financially supported by National Natural Science Foundation (NNSF) of China, the Government of Guangdong Province and Guangzhou City (Nos. U0734002, 50872158, 10774195, 8251027501000010 and 10C22051347), and the China Postdoctoral Science Foundation (No. 20080440117). W.Z.Z thanks the Royal Society for financial support to an International Collaboration project in this field.

Supporting Information Available: Structural description of the orthorhombic unit cell and the pseudocubic subcell of $CaTiO_3$. This material is available free of charge via the Internet at http://pubs.acs.org.

JA106461U

(19) (a) Curie, P. *Bull. Soc. Fr. Mineral. Cristallogr.* **1885**, *8*, 145–150. (b) Wulff, G. *Z. Kristallogr.* **1901**, *34*, 449–480.